

Article

Anatomy student grade prediction method based on multimodal model for reconstruction of human biomechanical endpoints

Chuang Cheng, Lihua Ma*

Chongqing Three Gorges Medical College, Chongqing 404120, China

* **Corresponding author:** Lihua Ma, 13066030@qq.com

CITATION

Cheng C, Ma L. Anatomy student grade prediction method based on multimodal model for reconstruction of human biomechanical endpoints. *Molecular & Cellular Biomechanics*. 2024; 21(4): 1012.
<https://doi.org/10.62617/mcb1012>

ARTICLE INFO

Received: 5 December 2024

Accepted: 19 December 2024

Available online: 30 December 2024

COPYRIGHT



Copyright © 2024 by author(s).

Molecular & Cellular Biomechanics

is published by Sin-Chn Scientific

Press Pte. Ltd. This work is licensed

under the Creative Commons

Attribution (CC BY) license.

<https://creativecommons.org/licenses/by/4.0/>

Abstract: Dissecting and studying the morphology of the tibial insertion point of the anterior cruciate ligament (ACL) of the knee joint, and using finite element analysis software to analyze the distribution of mechanical insertion points of the ACL, providing a new concept for clinical ACL reconstruction. **Method:** Ten fresh adult knee joint specimens were selected, including six males and four females. The joint cavity was opened using a standard medial patellar approach, exposing and dissecting the ACL. The morphology of the ACL tibial insertion point was observed and recorded, and the anterior posterior and lateral diameters of the tibial insertion point were measured. Using 3D reconstruction software to simulate clinical physical examination Laehman test and pivot shift test, observe the force distribution of ACL at the tibial and femoral end insertion points, and finally construct a multiple stepwise regression model to evaluate students' classroom learning behavior and performance in this experiment. **Result:** The dense insertion point of the ACL tibia appears as a flattened and elongated arc shape, with an anterior posterior diameter of (13.8 ± 2.0) mm, a body lateral diameter of (5.3 ± 0.6) mm, and a leading edge lateral diameter of (11.5 ± 1.2) mm. Finite element analysis shows that the area of high stress at the femoral end is an elliptical region near the resident's ridge, while the area of high stress at the tibial end is elongated along the medial intercondylar ridge, which is consistent with anatomical observations and theoretically confirms the biomechanical distribution characteristics of ACL insertion points. On the other hand, some learning behaviors of students have a positive impact on their academic performance. **Conclusion:** Anatomical studies and finite element analysis have confirmed that the tibial insertion point of ACL is a flattened and elongated arc. The ideal ACL reconstruction technique should be based on its biomechanical characteristics. Based on biomechanical analysis, the concept of anterior cruciate ligament biomechanical insertion point reconstruction is proposed. Using a multiple stepwise regression model to predict students' academic performance can improve the effectiveness of teaching activities and provide scientific basis for teaching research and reform.

Keywords: biomechanics; human anatomy; stepwise regression; learning behavior; performance evaluation model

1. Introduction

The anterior cruciate ligament (ACL) is one of the most crucial stabilizing structures in the knee joint. It plays a key role not only in preventing anterior displacement of the tibia but also contributes to the rotational stability of the knee. ACL injuries are common sports-related injuries, particularly among athletes involved in activities that require rapid changes in direction or sudden stops. Following an ACL injury, patients often experience knee instability, pain, and functional impairment. If left untreated or improperly managed, long-term complications may lead to secondary osteoarthritis. ACL reconstruction surgery is currently the primary method for treating

ACL ruptures, aiming to restore knee stability and function. Traditional ACL reconstruction techniques mainly focus on anatomical positioning, using autografts or allografts fixed to the tibia and femur to mimic the function of the native ACL. However, these techniques often overlook the study and reconstruction of the morphological features of the ACL insertion sites, resulting in an inability to fully restore postoperative knee biomechanical properties.

In recent years, with advancements in the anatomical study of the ACL, scholars have discovered that the ACL's direct insertion site on the tibia is narrowly arched or "C" shaped, while the femoral insertion site resembles an elliptical shape. These findings suggest that traditional circular bone tunnels may not be the optimal method for reconstruction. Consequently, international researchers have attempted to use various shaped bone tunnels, such as gourd-shaped, rectangular, and elliptical, to simulate the anatomical morphology of the ACL insertion sites. Although these studies are theoretically innovative, they still face certain limitations in surgical technique implementation.

The anterior cruciate ligament (ACL) is an essential structure for maintaining the normal movement of the knee joint. Its injury can compromise knee stability, affect joint function, and lead to secondary osteoarthritis. Anatomical reconstruction of the ACL is currently considered the gold standard for treating ACL ruptures. However, mainstream ACL reconstruction techniques focus primarily on anatomical positioning, often overlooking the study and reconstruction of the insertion site morphology. Recent domestic and international anatomical studies on the ACL have revealed that its tibial direct insertion site is narrowly arcuate or "C"-shaped, while the femoral direct insertion site resembles an oval shape. Due to traditional concepts and surgical method limitations, clinical applications of ACL reconstruction typically use round bone tunnels made with bone drills matching the graft's thickness, which cannot effectively restore the biomechanical properties of the ACL. Reconstruction techniques simulating the anatomical morphology of the ACL insertion sites have emerged. International scholars have attempted to reconstruct tibial or femoral bone tunnels using shapes like gourd, rectangular, and oval [1], but these studies have their own limitations in surgical techniques. Since 2014, the Institute of Sports Medicine at Peking University Third Hospital has been researching reconstruction techniques that simulate the morphology of ACL insertion sites, continuously improving surgical techniques and completing animal experiments and clinical follow-up studies on oval bone tunnel reconstruction techniques. With the advancement of concepts and a deeper understanding of ACL anatomy, this study uses knee specimens to further observe the morphological characteristics of the ACL's tibial mechanical insertion point. It also employs finite element analysis to examine the force characteristics of the ACL's tibial and femoral insertion points, providing new insights for clinical ACL reconstruction.

2. Materials and methods

2.1. Anatomical study

Selection of 10 fresh adult Chinese knee joint specimens for gross observation and measurement of the ACL tibial insertion site, with 6 males and 4 females. The selection criteria excluded joints with significant knee degenerative changes and

anatomical abnormalities, ensuring complete joint capsule and ligament structures. This study was approved by the Ethics Committee of Peking University Third Hospital before commencement, strictly following the ethical standards for human specimen research. A standard medial parapatellar approach was adopted, carefully removing the muscles around the knee joint, the joint capsule, and the patella, while preserving the cruciate ligaments and meniscus. The fat and synovium around the ACL were removed due to the close anatomical relationship between its tibial insertion site and the anterior horn of the lateral meniscus. The ACL was gradually separated from inside to outside, peeling off from the tibial insertion site, while simultaneously tracing the contour of the insertion site for gross observation of its morphology. A digital caliper (precision 0.01 mm, Shanghai Macro International Trade Co., Ltd.) was used to measure the anteroposterior diameter (a) and mediolateral diameter of the tibial insertion site, where the mediolateral diameter included the body's mediolateral diameter (b) (**Figure 1**).

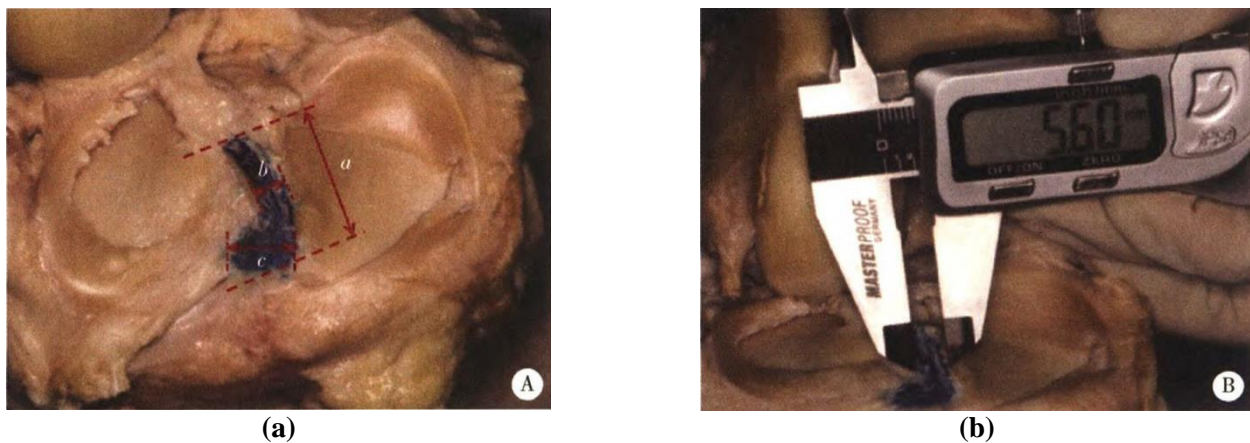


Figure 1. Specimen measurement. (a) anterior cruciate ligament (ACL) tibial insertion extent; (b) width measurement of midsubstance of ACL tibial insertion with vernier caliper.

A, anterior cruciate ligament (ACL) tibial insertion extent; B, width measurement of midsubstance of ACL tibial insertion with vernier caliper; a, the anterior-posterior diameter of ACL tibial insertion; b, the width of midsubstance of ACL tibial insertion.

2.2. Results of finite element analysis

Finite Element Analysis (FEA) is a numerical simulation method that discretizes a continuous physical structure into multiple small elements and solves approximate solutions on these elements. This method is widely used in engineering and scientific fields to predict the mechanical behavior of complex structures. The basic principle of finite element analysis is to decompose a complex problem into multiple simple sub problems, each of which is solved in a smaller area. By independently calculating each subregion and combining all results, an approximate solution to the entire problem is obtained. In finite element analysis, the solution domain first needs to be divided into several small, regularly shaped elements, such as triangles or quadrilaterals. This process is called grid partitioning. The quality of the grid directly affects the accuracy and efficiency of the calculation results. When conducting finite element analysis, it is necessary to set appropriate boundary conditions and loading conditions. Boundary

conditions are used to limit the degrees of freedom of the model, while loading conditions simulate external forces in actual work. The setting of these conditions has a significant impact on the analysis results. By establishing and solving algebraic equations, parameters such as displacement and stress at each node can be obtained. The post-processing stage includes visualizing and interpreting the results, helping engineers understand the behavior of the model and make corresponding design improvements.

Choosing appropriate samples is crucial as they will directly affect the reliability and validity of research results. The main considerations are as follows:

(1) Representativeness: The selected sample should be able to represent the typical anatomical features of the target population. For example, when studying ACL reconstruction, individuals with specific age, gender, weight, and activity levels may be selected.

(2) Consistency: In order to reduce variability and improve the reliability of results, a set of samples with similar anatomical features is usually selected. This helps ensure that the observed effects are caused by the surgical technique itself, rather than individual differences.

(3) Sufficient quantity: A sufficient number of samples can improve the effectiveness of statistical analysis and help distinguish between true effects and accidental errors.

(4) Quality control: All samples should undergo strict quality control to ensure that they are free from diseases or other factors that may affect the results. This study utilized three-dimensional thin-layer magnetic resonance imaging (MRI) scans of normal knee joints (slice thickness 0.7 mm, resolution 256×256 , medie3d sag mm \times 0.7 mm). The three-dimensional reconstruction software MIMICS was used to create a three-dimensional model of the knee joint. Subsequently, the finite element analysis software ANSYS was employed to establish a human knee joint finite element model, including the femur, tibia, fibula, anterior cruciate ligament (ACL), posterior cruciate ligament (PCL), medial collateral ligament (MCL), and lateral collateral ligament (LCL). Boolean operations were performed to establish fixed connections between the ligaments and their bony attachment points. One of the primary functions of the ACL is to restrict anterior translation and axial rotation of the tibia [2,3]. Therefore, this study simulated clinical physical examinations: the Lachman test and the pivot-shift test, analyzing the stress distribution characteristics at the ACL insertion sites on the femur and tibia. For the Lachman test loading conditions: the proximal and middle nodes of the femur were completely fixed, the tibia and fibula were set as bounded contact, restricting flexion and extension movements of the tibia and fibula, with a forward force of 134 N applied to the proximal tibia. For the pivot-shift test loading conditions: the proximal and middle nodes of the femur were completely fixed, the tibia and fibula were set as relatively bounded fixed, with a valgus moment of 10 Nm and an internal rotation moment of 5 Nm applied to the tibia, restricting flexion and extension movements of the tibia and fibula. Bone tissue material properties were set with an elastic modulus of 17 GPa and a Poisson's ratio of 0.36; ligament tissue material properties were set with an elastic modulus of 390 MPa and a Poisson's ratio of 0.49. The ANSYS software was used for solving and analyzing the stress distribution characteristics at the ACL insertion sites on the tibia and femur.

3. Results

3.1. Gross anatomy of the ACL tibial insertion site

The gross observation of the ACL tibial insertion site shows an elongated, curved shape without any obvious division into bundles. The dense fibers run anteriorly along the medial intercondylar eminence, crossing over the insertion point of the anterior horn of the lateral meniscus and terminating in front of it. The anterior edge can reach the bony landmark known as the anterior ridge (**Figure 1**). The measured anteroposterior diameter of the ACL tibial insertion site is (13.8 ± 2.0) mm, with the body's mediolateral diameter being (5.3 ± 0.6) mm, and the anterior edge's mediolateral diameter being (11.5 ± 1.2) mm.

3.2. Performance prediction

The stress distribution at the ACL insertion sites on the tibia and femur during the Lachman test and pivot-shift test is shown in **Figure 2**. On the femoral side, the area with higher stress is near the residents' ridge in an elliptical region. On the tibial side, the area with higher stress extends along the medial intercondylar ridge in a narrow, elongated distribution, consistent with anatomical observations. This theoretically verifies the biomechanical distribution characteristics of the ACL insertion sites.

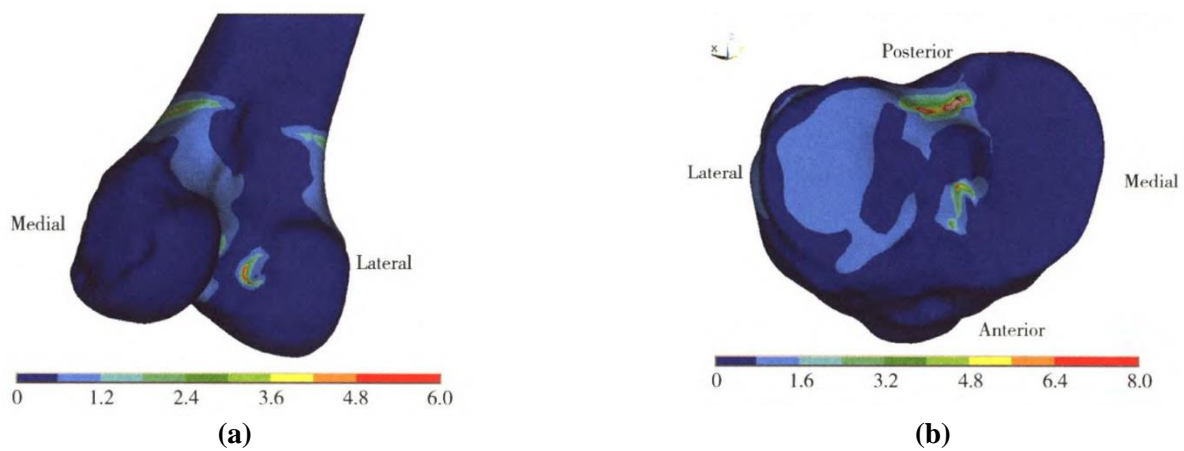


Figure 2. von mises stress distribution on the femoraside and tibial side with pivot-shift test. (a) femoraside; (b) tibial side.

4. Discussion

4.1. Anatomy and finite element analysis of the ACL tibial insertion site

International recent anatomical studies on the ACL tibial insertion site indicate that it is divided into a direct insertion and an indirect insertion. The direct insertion forms a “C” shape with an average length of (12.6 ± 2.3) mm and width of (3.3 ± 0.4) mm, with an average area of (31.4 ± 7.2) mm². The indirect insertion consists of fan-shaped fibers with an average area of (79.6 ± 12.7) mm². Together, the direct and indirect insertions form a “duck-foot” shape. Yuda et al. conducted an anatomical study on the ACL tibial insertion site in domestic adults and found that the direct

insertion is arc-shaped, starting from the outer side of the medial intercondylar eminence and ending in front of the anterior horn of the lateral meniscus, with a width of (11.2 ± 2.4) mm and thickness of $(3.0\text{--}4.0 \pm 0.3)$ mm, and a cross-sectional area of (28.8 ± 7.8) mm². The complete tibial insertion has a left-right diameter of (9.5 ± 1.8) mm, anteroposterior diameter of $(15.0 \pm 1.9 \pm 0.6)$ mm, and a cross-sectional area of (117.8 ± 12.2) . The ACL tibial insertion site observed in this study matches the description of the direct insertion in the above studies, while the coverage area of the indirect insertion has sparse fibers. The ACL tibial insertion site has a close relationship with the anterior horn of the lateral meniscus, and traditional ACL reconstruction can easily cause iatrogenic damage to this region. Reconstructing the ACL at the direct insertion point theoretically avoids damage to the anterior horn of the lateral meniscus. This study only conducted an anatomical investigation of the tibial insertion point, and there is relatively less controversy regarding the elliptical shape of the femoral insertion point. Our research group previously observed the morphology of the femoral insertion point in 30 formalin-fixed adult knee specimens. The biomechanical insertion points of the femur and tibia are theoretically the main sites that bear the mechanical stress of anterior translation and rotational forces of the knee joint. To verify this hypothesis, this study used finite element analysis software to create a knee joint model and applied stresses of forward (134 N), internal rotation moment (10 Nm), and valgus rotation (valgus moment 5 Nm). The stress distribution solution found that the concentrated areas of mechanics were consistent with anatomical observations, which may bring new insights and technical innovations for clinical ACL reconstruction. This study model is based on three-dimensional MRI images, providing high geometric similarity for both ligaments and bone tissues. The limitations of finite element analysis include simplifying the bones and ligaments using a linear elastic material model and not including articular cartilage and menisci in the model, necessitating further in-depth research. However, considering that this study simulated Lachman and pivot-shift tests, where the ACL bears 87% of the force in restricting tibial anterior translation [4], and the aim of this study was to analyze the stress concentration areas (biomechanical insertion points) on the femur and tibia, this simplification can be temporarily ignored regarding its impact on the research results.

4.2. Concept of biomechanical insertion point reconstruction

Based on the latest anatomical studies and finite element analysis results, this study proposes modifying the tibial bone tunnel to a flat, elongated oval shape while retaining the elliptical biomechanical endpoint for femoral bone tunnel reconstruction (biomechanical section reconstruction, BIR). The schematic diagram of the bone tunnel cross-section is shown in **Figure 3**. Assuming that both the traditional circular bone tunnel and the modified bone tunnel perfectly match the graft, the two bone tunnel cross-sectional areas are equal. Therefore, the theoretical value can be calculated using the area formula. Let D represent the diameter of the circular bone tunnel, Maj represent the major axis of the bone tunnel, and Min represent the minor axis. According to the area formula $S_{Circular} = \pi \left(\frac{D}{2}\right)^2$, $S_{flat-oval} = \pi \left(\frac{Min}{2}\right)^2 + (Maj - Min) \times Min$, $S_{elliptical} = \pi \left(\frac{Maj \times Min}{4}\right)$, The relationships between the major

and minor axes of the tibial bone tunnel and the diameter of the circular bone tunnel can be calculated as follows:

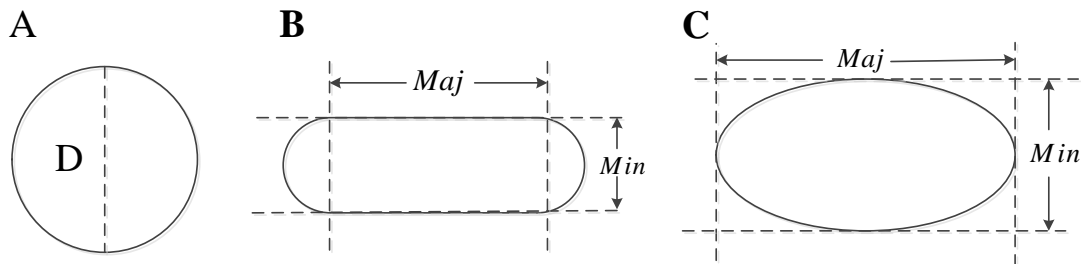


Figure 3. Sectional sketch view of bone tunnel.

$Maj = \frac{\pi(D^2 - Min^2)}{4Min}$ The relationships between the major and minor axes of the femoral bone tunnel and the diameter of the elliptical bone tunnel can be calculated as follows: $D^2 = Maj \times Min$, These can be compiled into a standardized data table for intraoperative reference.

A, sectional view of round bone tunnel; B, sectional view of rounded-rec-tangle tibial tunnel of ACL-BIR; C, sectional view of oval femoral tunnel of ACL-BIR.

Tensho et al., through anatomical studies on 12 pairs of knee joint specimens, found that the anterior-medial boundary of the ACL tibial insertion point can be referenced to the “L” shaped ridge formed by the anterior ridge and the intercondylar ridge of the medial condyle, while the lateral boundary can refer to the anterior horn of the lateral meniscus. In the ACL-BIR concept, the flat-oval bone tunnel for the tibia is positioned using the reverse “L” shaped ridge formed by the anterior ridge and the intercondylar ridge as a bony landmark. To prevent individual variability, it can also refer to the relationship with the free edge of the anterior horn of the lateral meniscus and the distance from the fibers in front of the PCL for confirmation. When positioning and drilling the tibial bone tunnel, select a smaller diameter bone tunnel drill according to the patient’s ACL tibial insertion point range and graft diameter. For example, when the graft diameter is 8 mm, generally use a 5 mm bone drill bit, depending on the shape of the patient’s ACL tibial insertion point; the narrower the insertion point, the smaller the diameter of the bone tunnel drill should be selected. After drilling through the bone tunnel, use a bone tunnel rasp to adjust according to the theoretical value of the flat-oval bone tunnel, and adjust the bone tunnel entrance to a flat-oval shape, with an adjustment depth of 10 mm, not affecting distal fixation. Use a proportional ruler under arthroscopy to assist measurement for standardization during surgery. The tibial bone tunnel is positioned using the anterior ridge and the intercondylar ridge of the medial condyle as bony landmarks, defining the anterior and medial boundaries of the tibial bone tunnel respectively. This can improve the accuracy and repeatability of the tibial bone tunnel positioning, ensuring the direction of the biomechanical insertion point of the reconstructed ACL, and maximizing the biomechanical function of the reconstructed ACL. Using a bone tunnel rasp as a tool for adjusting the bone tunnel can reduce the risk of inner wall fractures of the bone tunnel. On the other hand, it allows for selective stepwise adjustment of the long axis of the bone tunnel based on theoretical values, meeting the needs for personalized biomechanical insertion point

reconstruction. Femoral bone tunnel positioning can be achieved through an anterior medial portal (AMP) or transtibial (TT) approach, combining the resident’s ridge and the distance between the remnants of the ACL femoral insertion point and the posterior edge of the articular cartilage of the outer condyle, usually at the position of ten or twelve o’clock on a clock face. The thickness of the posterior wall after drilling is 1–2 mm. Generally, a 6 mm femoral bone tunnel positioner is used to position the femoral bone tunnel, with radiofrequency marking the positioning points, penetrating guide pins, and a 4.5 mm hollow drill bit drilling through the lateral cortex of the femur to measure the length of the femoral bone tunnel at the femoral end. Based on the patient’s ACL femoral insertion point range and graft diameter, select a smaller diameter hollow drill bit. However, since the femoral insertion point is not as narrow and long as the tibial insertion point, there is no need to prepare a bone tunnel with a large aspect ratio. For example, when the graft diameter is 8 mm, generally use a 6 mm bone drill bit to drill a coarse bone tunnel, then use a bone tunnel rasp according to the theoretical value of the elliptical bone tunnel, adjusting the bone tunnel entrance to an elliptical shape with an adjustment depth of 10 mm, not affecting distal fixation. During surgery, also use a proportional ruler under arthroscopy to assist in achieving standardization.

4.3. Analysis of student learning situation

4.3.1. Data sources and research methods

Taking the human anatomy course offered by Chongqing Three Gorges Medical College as an example, we exported classroom learning behavior data and final exam scores for five classes from the 2017–2019 cohorts to form the model group. The classroom learning behavior data for two classes from the 2020 cohort were used as the prediction group. As shown in **Figure 4**, using student classroom learning behavior data as independent variables and final exam scores as dependent variables, this study explores the main factors affecting academic performance under digital teaching. We aim to construct a model linking classroom learning behaviors with performance assessment to predict students’ final exam scores.

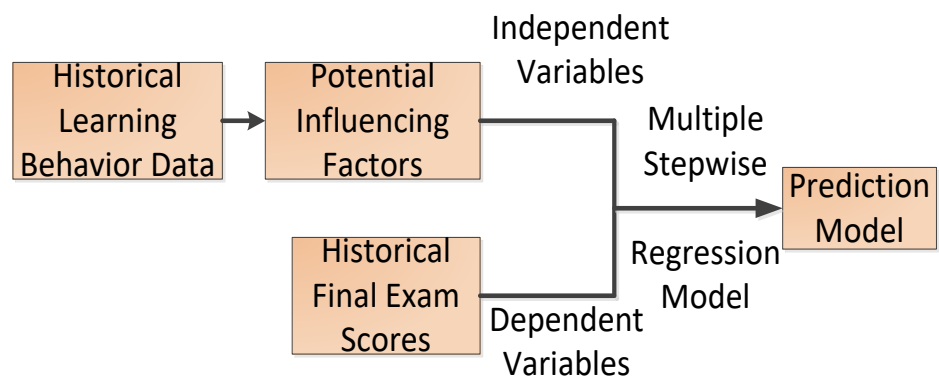


Figure 4. Prediction model building approach.

The study reviewed the learning behavior data of students from seven classes in both the model group and prediction group, categorizing these behaviors into three main types (see **Table 1**): learning resources, classroom interaction, and student performance. Learning resources encompass video and non-video materials;

classroom interaction includes activities such as check-ins, quizzes, light live discussions, brainstorming sessions, polls, homework/group tasks; student performance comprises classroom participation and teacher endorsements.

Table 1. Construction of indicators affecting student performance.

Class I	Class II	Symbol
Learning Resources	Video Resources	video, V
	Non-video Resources	non video, NV
Classroom Interaction	Check-in	sign in, S
	Quiz/Test	test, T
	Light Live Stream-Discussion	discuss, D
	Brainstorming	brainstorming, B
	Polling/Survey	voting questionnaire, VQ
Student Performance	Homework/Group Task	homework/group tasks, HT
	Classroom Performance	performance, P
	Praised by the Teacher	likes, L

4.3.2. Analytical methods

(1) forward method

The forward method involves establishing univariate regression models between each of the n independent variables X_1, X_2, \dots, X_n and the dependent variable Y .

$$Y = \beta_0 + \beta_i X_i + \varepsilon \quad i = 1, 2, \dots, n$$

Perform an F -test on each equation to identify the maximum F -value, i.e., $F_{1\max} = \max \{F_{11}, F_{12}, \dots, F_{1n}\}$. Introduce the corresponding variable X_i into the model and repeat this step until no more variables are introduced.

(2) backward method

The backward method, which is the opposite of the forward method, involves initially including all independent variables $X \in \{X_1, X_2, \dots, X_n\}$ in the model. Each variable is then subjected to an F -test to identify the minimum F -value, i.e., $F_{1\min} = \min \{F_{11}, F_{12}, \dots, F_{1n}\}$. If $F_{1\min} < F_0$ (the critical value), the corresponding independent variable is removed. This process continues, gradually eliminating independent variables that have no significant impact on the dependent variable, until no more variables can be removed.

(3) multivariate stepwise regression

The multivariate stepwise regression model combines both forward and backward methods. The idea is to introduce a set of candidate variables into the model one by one, performing F -tests on the newly introduced variables and t -tests on the already included variables. The model automatically eliminates insignificant variables and selects and retains variables that have significant influence and do not suffer from severe multicollinearity to construct the regression model.

4.3.3. Analysis of influencing factors

The study employed multivariate stepwise regression analysis to examine the

final exam scores and classroom learning behavior data of five classes from the Chongqing Three Gorges Medical College for the 2017–2019 cohorts. The diagnostic results of the stepwise regression model indicated: (1) A Variance Inflation Factor (VIF) < 5 suggests that there is no multicollinearity in the model; (2) Durbin-Watson (D-W) values close to 2 indicate no autocorrelation between samples, confirming that the model does not suffer from autocorrelation issues; (3) An *F*-test with $p < 0.05$ indicates that the model passes the *F*-test.

Based on the results of multivariate stepwise regression analysis (see **Table 2**), all five models meet the diagnostic criteria, indicating that they are well-constructed. The models are as follows:

$$\text{Model 1: Final Exam Score} = 59.022 + 0.294 \times T + 0.091 \times B$$

$$\text{Model 2: Final Exam Score} = 46.434 + 0.224 \times T + 0.053 \times B$$

$$\text{Model 3: Final Exam Score} = 39.367 + 0.447 \times T$$

$$\text{Model 4: Final Exam Score} = 41.092 + 0.392 \times T + 0.180 \times L$$

$$\text{Model 5: Final Exam Score} = 55.394 + 0.211 \times T + 0.147 \times D$$

Table 2. Results of multiple stepwise regression analysis.

Model	Unstandardized Coefficients		Standardized Coefficients	<i>t</i>	<i>p</i>	Collinearity Diagnostics		
	B	Standard Deviation	Beta			VIF	Tolerance	
1	constant	59.022	8.630	-	6.839	0.000**	-	-
	T	0.294	0.108	0.238	2.721	0.008**	1.017	0.983
	B	0.091	0.040	0.199	2.266	0.025*	10.17	0.983
	<i>F</i>	$F(2, 118) = 7.192, p = 0.01$						
	<i>D-W</i>	2.317						
2	constant	46.434	4.339	-	10.703	0.000**	-	-
	T	0.224	0.061	0.400	3.675	0.000**	1.354	0.739
	B	0.053	0.025	0.232	2.135	0.036*	1.354	0.739
	<i>F</i>	$F(2, 79) = 17.659, p = 0.000$						
	<i>D-W</i>	2.195						
3	constant	39.367	16.462	-	2.391	0.021*	-	-
	T	0.447	0.177	0.336	2.525	0.015*	1.000	1.000
	<i>F</i>	$F(1, 50) = 6.373, p = 0.015$						
	<i>D-W</i>	1.772						
4	constant	41.092	10.302	-	3.989	0.000**	-	-
	T	0.392	0.114	0.413	3.430	0.001**	1.021	0.979
	L	0.180	0.089	0.245	2.035	0.047*	1.021	0.979
	<i>F</i>	$F(2, 52) = 9.154, p = 0.000$						
	<i>D-W</i>	1.696						
5	constant	55.394	9.884	-	5.604	0.000**	-	-
	T	0.211	0.104	0.268	2.028	0.049*	1.039	0.963
	D	0.147	0.050	0.388	2.943	0.005**	1.039	0.963
	<i>F</i>	$F(2, 44) = 7.828, p = 0.001$						
	<i>D-W</i>	1.779						

Dependent Variable: Final exam scores; * $p < 0.05$ ** $p < 0.01$.

Based on the above stepwise regression models, it is found that: (1) In Models 1 and 2, testing and brainstorming classroom behaviors have a significant positive impact on students' final exam scores; (2) In Model 3, only testing has a significant positive impact on students' final exam scores; (3) In Model 4, the classroom behaviors affecting final exam scores include testing and receiving likes from teachers; (4) In Model 5, testing and light live streaming—discussion have a significant positive impact on final exam scores. Overall, certain classroom learning behaviors such as testing, brainstorming, and light live streaming—discussion have a significant positive impact on academic performance.

4.3.4. Performance prediction

Student exam performance prediction is about anticipating potential risks in students' human anatomy course grades, allowing teachers to understand students' learning situations and grade warning levels in advance. This enables real-time adjustment of classroom teaching activities and the formulation of personalized, rationalized learning goals based on warning levels. It guides students to actively participate in classroom activities and improves the rate of effective student learning [5–7]. According to the five models described [8,9], we predicted the academic performance of two classes of 2020 students. The predicted scores below 70 points were categorized into high, medium, and low risk levels. **Figure 5** shows that Class 1 had 12 students at high risk with a probability of 60%; 7 students at medium risk with a probability of 40%; and 10 students at low risk with a probability of 20%. In Class 2, there were 8 students at high risk, with 2 students having a probability of 80% and 6 students having a probability of 60%; 5 students were at medium risk with a probability of 40%; and 5 students were at low risk with a probability of 20%.

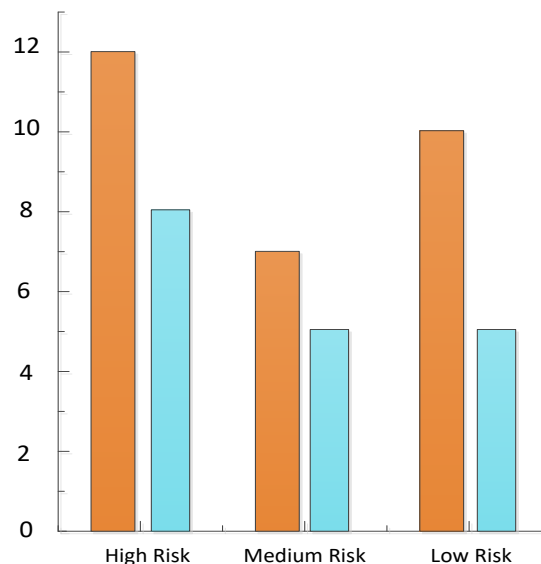


Figure 5. Prediction results for group with scores below 70.

4.3.5. Adjustment of teaching plans

Following the principle [10,11] of “performance prediction—risk grading—differentiated adjustment—improvement of performance,” teaching plans are adjusted based on the actual learning behaviors of students at high, medium, and low risk levels

[12–14]. As shown in **Figure 6**, the specific content mainly includes: pre-class preparation materials [9], classroom teaching activities, and assignment of homework after class [15–17]. Predictions are carried out by chapter to facilitate timely attention to students’ learning needs and adjustment of teachers’ teaching plans [18–21]. The overall principle is to be guided by the learning needs of the majority group, supplemented by the learning characteristics of the minority group, ultimately achieving differentiated teaching that takes individual differences into account and aims to comprehensively improve student learning outcomes [22–25].

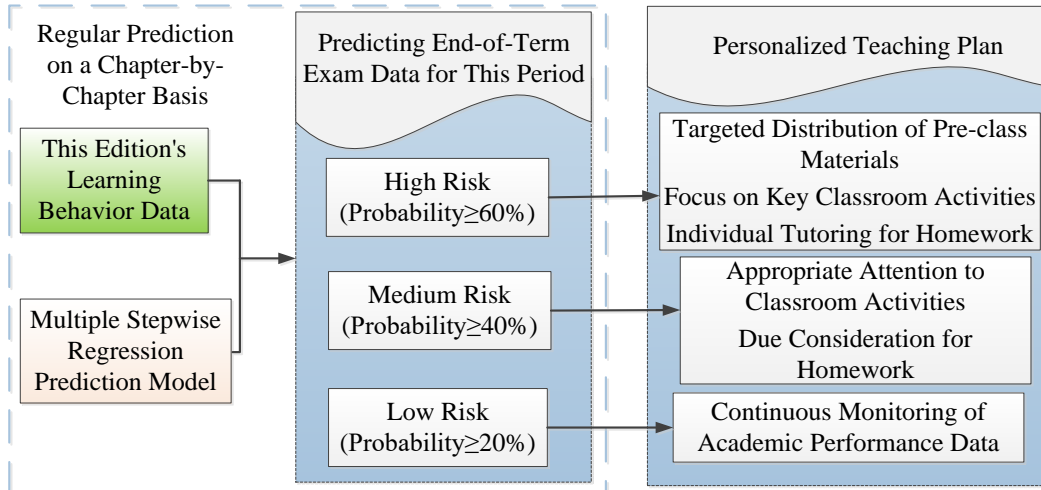


Figure 6. Personalized teaching pathway.

In the spring semester of 2023 [26–28], this method was applied to adjust teaching for two classes (prediction group) of the Surveying and Mapping 2020 cohort [29,30]. As shown in **Figure 7**, compared to the class of 2019, the performance of the class of 2020 improved significantly, with an average score increase of 5.58 points.

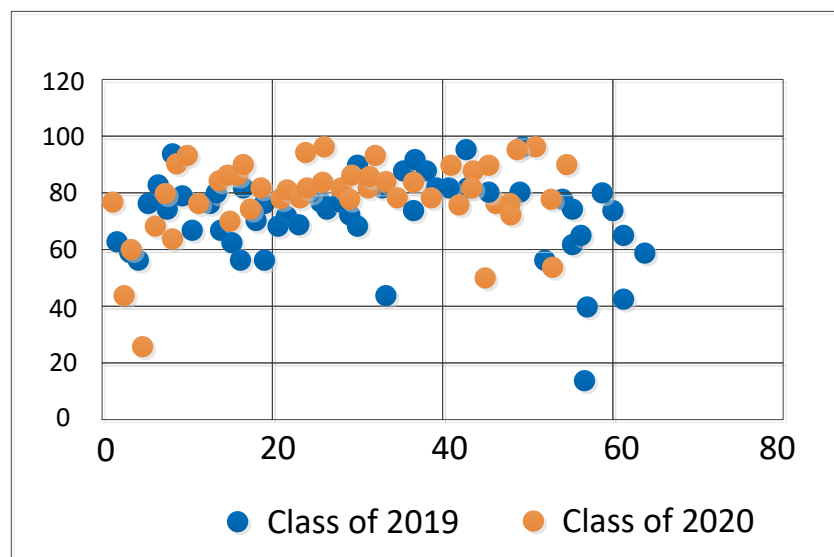


Figure 7. Comparison of final exam results between the class of 2020 and the class of 2019.

5. Conclusion

Anatomical research was conducted to observe the morphology of the anterior cruciate ligament (ACL) tibial insertion point in the knee joint, and finite element analysis software was used to analyze the mechanical insertion point distribution of ACL, providing a new concept for clinical ACL reconstruction. Three dimensional reconstruction software MIMICS and finite element analysis software ANSYS were used to establish a knee joint model, simulate clinical physical examination Laehman test and pivot shift test, and observe the force distribution of ACL at the tibial and femoral end insertion points. The results showed that the dense insertion point of ACL tibia appeared as a flattened and elongated arc shape, with an anterior posterior diameter of (13.8 ± 2.0) mm, a body left and right diameter of (5.3 ± 0.6) mm, and a leading edge left and right diameter of (11.5 ± 1.2) mm. Finite element analysis shows that the area of high stress at the femoral end is an elliptical region near the resident's ridge, while the area of high stress at the tibial end is elongated along the medial intercondylar ridge, which is consistent with anatomical observations and theoretically confirms the biomechanical distribution characteristics of ACL insertion points.

In summary, both anatomical observation and finite element analysis in this study confirm that the ACL tibial insertion point is a flat elongated arc, and ideal ACL reconstruction techniques should be based on its biomechanical characteristics. The ACL-BIR concept simulates the biomechanical insertion point morphology of the ACL, thereby changing the overall shape of the graft to maximize biomechanical function, making the graft's biomechanical properties closer to those of the original ACL. This provides a new concept for clinical ACL reconstruction with good prospects for clinical application. Then we use multiple stepwise regression models to analyze and identify classroom learning behaviors that can enhance student performance. This provides substantive suggestions for educational reform. By predicting student exam scores through the model, teachers can identify high-risk, medium-risk, and low-risk students, allowing them to set targeted and differentiated learning goals for students, avoiding potential "red line warning" crises. Timely intervention for high-risk students based on prediction results, by improving their classroom learning behaviors and academic performance, helps ensure the achievement of educational objectives and enhances the quality of talent cultivation.

Author contributions: Conceptualization, CC and LM; methodology, CC; software, CC; validation, CC and LM; formal analysis, CC; investigation, LM; resources, LM; data curation, CC; writing—original draft preparation, LM; writing—review and editing, CC; visualization, CC; supervision, LM; project administration, CC; funding acquisition, CC. All authors have read and agreed to the published version of the manuscript.

Ethical approval: The study was conducted in accordance with the Declaration of Helsinki, and approved by the Chongqing Three Gorges Medical College's Medical Ethics Committee (11 May 2023).

Conflict of interest: The authors declare no conflict of interest.

References

1. Ma Jing, Jin Yanchi, Yang Yang, et al. Educational Metaverse: System Construction and Practical Application of a New Form of Internet Education. *Modern Educational Technology*, 2023, 33(7): 99-107.
2. Chen Li, Guo Yujuan, Zhang Wenmei. The Worldview of “Internet + Education”: A Complex Systems Perspective. *China Distance Education*, 2023, 43(8): 7-12.
3. Zhang Xiumei, Tian Tian, Tian Mengmeng, et al. Evolution and Trends of Smart Teaching Research in China over the Past Decade. *China Distance Education (Comprehensive Edition)*, 2020(9): 62-69.
4. Cheng Gang, Yang Jie, Wang Lei, et al. Comprehensive Reform and Practice of the Human anatomy course on “Principles and Applications of Geographic Information Systems” under the Smart Teaching Environment. *Bulletin of Surveying and Mapping*, 2021(12): 158-162.
5. Qiu Xiaoyan, Xiao Xiong. Practice and Exploration of the “Smart Classroom” Teaching Model in Cell Biology. *Chinese Journal of Cell Biology*, 2021, 43(12): 2377-2381.
6. Zhang Sheng, Zhao Jue. Visualization Research on Smart Education Management System: A Case Study of Hunan University of Technology and Business. *Modern Educational Technology*, 2020, 30(8): 80-85.
7. Yu Tai, Li Li, Zhao Xin. Construction of Smart Teaching Environment in Higher Education Based on Educational Big Data. *Laboratory Research and Exploration*, 2020, 39(7): 285-288.
8. Lin Xiuyu, Li Mengjie. Theoretical Model and Mechanism of Learning Analytics in Smart Learning Environments. *Modern Educational Technology*, 2019, 29(4): 16-22.
9. Tan Jisheng. Research on the Implementation Strategy of Smart Teaching Mode in Higher Education under the Background of Educational Informatization. *Journal of Qilu Normal University*, 2021, 36(6): 29-34.
10. Miao Qijun. Exploration of Mixed Teaching Mode for Accounting Human anatomy courses under the “Internet +” Background: A Practice Based on the Lanmo Cloud Class Platform. *Finance & Accounting Monthly*, 2017(33): 78-83.
11. Liu M, Qian F, Mi J, et al. Biomechanical energy harvesting for wearable and mobile devices: State-of-the-art and future directions. *Applied Energy*, 2022, 321: 119379.
12. Ji S, Ghajari M, Mao H, et al. Use of brain biomechanical models for monitoring impact exposure in contact sports. *Annals of Biomedical Engineering*, 2022, 50(11): 1389-1408.
13. Alsaeed R, Hassn Y, Alaboudi W, et al. Biomechanical analytical study of some obstacles affecting the development of football players. *International Journal of Physical Education, Sports and Health*, 2023, 10(3): 342-346.
14. Widmer J, Cornaz F, Scheibler G, et al. Biomechanical contribution of spinal structures to stability of the lumbar spine—novel biomechanical insights. *The Spine Journal*, 2020, 20(10): 1705-1716.
15. Gupta V, Singla R, Singh G, et al. Development of Soft Composite Based Anisotropic Synthetic Skin for Biomechanical Testing. *Fibers*, 2023, 11(6): 55.
16. Aguilar-Sánchez A, Li J, Jalvo B, et al. Understanding the effect of different nanocelluloses on the proliferation and biomechanical properties of *E. coli*. *Cell Reports Physical Science*, 2024, 5(10).
17. Fray M, Davis K G. Effectiveness of safe patient handling equipment and techniques: A review of biomechanical studies. *Human Factors*, 2024, 66(10): 2283-2322.
18. Singh G, Chanda A. Development and biomechanical testing of artificial surrogates for vaginal tissue. *Advances in Materials and Processing Technologies*, 2023: 1-11.
19. Guo Y, Yan T, Gao H, et al. High-strength fibrous sensors with an enhanced aggregate state for biomechanical monitoring of the Achilles tendon. *Journal of Materials Chemistry B*, 2024, 12(41): 10605-10615.
20. Hasan M D R, Ray R K, Chowdhury F R. Employee performance prediction: An integrated approach of business analytics and machine learning. *Journal of Business and Management Studies*, 2024, 6(1): 215-219.
21. Li M, Wang S, Gao H, et al. Selective removal of antibiotics over MgAl₂O₄/C₃N₄/YMnO₃ photocatalysts: Performance prediction and mechanism insight. *Journal of the American Ceramic Society*, 2023, 106(4): 2420-2442.
22. Gao Y, Gu X, Zhang H, et al. Runtime performance prediction for deep learning models with graph neural network[C]//2023 IEEE/ACM 45th International Conference on Software Engineering: Software Engineering in Practice (ICSE-SEIP). IEEE, 2023: 368-380.

23. Ming W, Sun P, Zhang Z, et al. A systematic review of machine learning methods applied to fuel cells in performance evaluation, durability prediction, and application monitoring. *International Journal of Hydrogen Energy*, 2023, 48(13): 5197-5228.
24. Pallathadka H, Wenda A, Ramirez-Asís E, et al. Classification and prediction of student performance data using various machine learning algorithms. *Materials today: proceedings*, 2023, 80: 3782-3785.
25. Batool S, Rashid J, Nisar M W, et al. Educational data mining to predict students' academic performance: A survey study. *Education and Information Technologies*, 2023, 28(1): 905-971
26. Adesina A A, Iyelolu T V, Paul P O. Leveraging predictive analytics for strategic decision-making: Enhancing business performance through data-driven insights. *World Journal of Advanced Research and Reviews*, 2024, 22(3): 1927-1934.
27. Sarvaiya J, Singh D. Prediction of performance parameters in friction stir processing using ANN and multiple regression models. *Materials Today: Proceedings*, 2023.
28. Mózes F E, Lee J A, Vali Y, et al. Performance of non-invasive tests and histology for the prediction of clinical outcomes in patients with non-alcoholic fatty liver disease: an individual participant data meta-analysis. *The Lancet Gastroenterology & Hepatology*, 2023, 8(8): 704-713.
29. Ogundepo E A, Yahya W B. Performance analysis of supervised classification models on heart disease prediction. *Innovations in Systems and Software Engineering*, 2023, 19(1): 129-144.
30. Wang L, Liu S, et al. Quantification of model uncertainty and variability for landslide displacement prediction based on Monte Carlo simulation. *Gondwana Research*, 2023, 123: 27-40.